

Article

Geological and Sedimentological Evidence of a Large Tsunami Occurring ~1100 Year BP from a Small Coastal Lake along the Bay of La Paz in Baja California Sur, Mexico

Terrence A. McCloskey *, Thomas A. Bianchette and Kam-biu Liu

Department of Oceanography and Coastal Sciences, School of the Coast and Environment, Louisiana State University, 1002Y Energy Coast and Environment Building, Baton Rouge, LA 70803, USA; E-Mails: tbianc1@tigers.lsu.edu (T.A.B.); kliu1@lsu.edu (K.L.)

* Author to whom correspondence should be addressed; E-Mail: tmccloskey@usgs.gov; Tel.: +1-727-502-8054.

Academic Editors: Valentin Heller and S. Bradley Moran

Received: 30 July 2015 / Accepted: 30 November 2015 / Published: 10 December 2015

Abstract: The importance of small-scale seismic events in enclosed water bodies, which can result in large tsunami waves capable of affecting comprehensive damage over small, geographically-confined areas are generally overlooked, although recognizing the occurrence of such events is a necessary element in adequately assessing the risk of natural hazards at specific locations. Here we present evidence for a probable large localized tsunami that occurred within the Bay of La Paz, Baja California Sur, ~1100 year before present (BP), which resulted in the creation of a shelly ridge at an elevation of ~2 m above mean high water (MHW). This ridge consists of a continuous wedge of poorly mixed marine sands and shells ~50 cm in depth deposited along the entire seaward edge of the lake. The marine shells collected from terrestrial environments around the lake include species from a variety of environments, including offshore species with minimum preferred depths of >13 m. The evidence suggests that this material was likely deposited by a tsunami with a runup of 2–3.6 m above MHW, probably associated with the slumping of an island along the tectonically active eastern edge of the bay.

Keywords: tsunami; Baja California; event deposit; coastal hazards

1. Introduction

Two recent events have focused attention on the hazards associated with supra-regional tsunamis generated by mega earthquakes occurring along major fault lines in the open ocean. On 26 December 2004 a rupture along the fault boundary between the Indo-Australian and Eurasian plates resulted in the 9.1 magnitude Sumatra-Andaman earthquake. The ensuing tsunami, that generated waves up to 30 m high, caused over 283,000 deaths in 14 countries [1,2]. On 11 March 2011, a 9.0 magnitude earthquake associated with a 450 km rupture of the Japan Trench generated a tsunami [3,4] that devastated Japan and achieved wave heights of 3.94 m as distant as the southern coast of Chile [5]. However, the risks associated with locally-generated tsunamis in confined water bodies have generally been ignored [6]. One example is the 1958 Lituya Bay, Alaska tsunami. Although this event was associated with a large earthquake on the Fairweather Fault, the proximal cause was a rockslide at the head of the bay that generated a tsunami that removed soil and vegetation up to a height of 524 m [7]. Miller [7] identified five occurrences of giant waves over the last 200 years in Lituya Bay indicating that in tectonically-active areas devastating localized tsunamis can occur over short return intervals, thereby posing large, but underappreciated, hazards for the immediate vicinity. Other large localized tsunamis associated with rockslides into confined bodies of water include events at Spirit Lake, Washington in 1980 (260 m runup) [8] and at the Vajont Reservoir, Italy in 1963 (260 m runup) [9,10]. The lack of focus on tsunami risks is problematic all along Mexico's west coast, but especially throughout the Baja Peninsula where the economies of coastal communities are largely tied to water-based tourism. The risk of localized events is of particular import within the semi-enclosed Bay of La Paz, given the presence of the city of La Paz in the shallow SW corner. Here we present geologic evidence from a small coastal lake on the margins of that bay, suggesting the possible occurrence of a tsunami at ~1100 year before present (BP).

2. Study Site

2.1. Geologic Setting

The Baja California (BC) Peninsula is rocky and dry, separated from the rest of Mexico by the Gulf of California. During the Mesozoic, when it was the western edge of both the continent and the North American plate, the BC Peninsula received volcanic detritus from calc-alkaline volcanoes farther to the east [11]. During the Oligocene and Miocene the volcanoes migrated west onto what is currently the east coast of the Baja Peninsula, depositing the Comondú Formation [11], at first in a shallow marine basin, then onto non-marine fans. Some subduction on the west coast of BC occurred at this point, terminating by ~10 million years ago (mya) [12]. Between 12 and 4 mya, as the North American Plate overrode the East Pacific Rise, Baja California slowly transferred onto the Pacific Plate as the plate boundary moved into the Gulf of California [13–15]. Although this is a right-lateral strike-slip boundary dominated by long transform faults and narrow spreading [16,17], the western edge of BC is part of the surrounding extensional province, characterized by normal faulting. The BC Peninsula as a whole has been being uplifted at ~0.1 m/kyr since 1 mya [18,19].

Our study site is located in the Bay of La Paz, located on the southern third of the peninsula; ~1000 km south of the Mexican/United States border (Figure 1). Hausback [11] identified the La Paz

Fault as a major NE-SW fault in the southern section of the peninsula, cutting across the entire peninsula just south of our study site. More recent studies have questioned the existence of this fault, and have instead identified the active normal San José del Cabo Fault as the dominant fault system [16]. North of this fault Coyan and others [17] have identified an array of active faults, the one closest to our site being the normal, northeast-dipping Saltito Fault, with scarp heights ranging from 7 to 14 m, which continues offshore. Saltito’s 14 km onshore rupture length corresponds to a magnitude (M) 6.5 earthquake [20]. Researchers working in the Bay of La Paz commonly identify a major buried fault along the western edge of the islands lying along the eastern edge of the bay [21,22]. The La Paz Basin is a half graben, controlled by the east-dipping Centenario Fault along its western edge [17]. Although the majority of regional earthquakes occur along the spreading axes in the center of the Gulf of California, a number of earthquakes >5.0 M have occurred in the Bay of La Paz since 1900 [16,21,22], with magnitude 7.0 events having an estimated occurrence interval of ~1000 years [22].

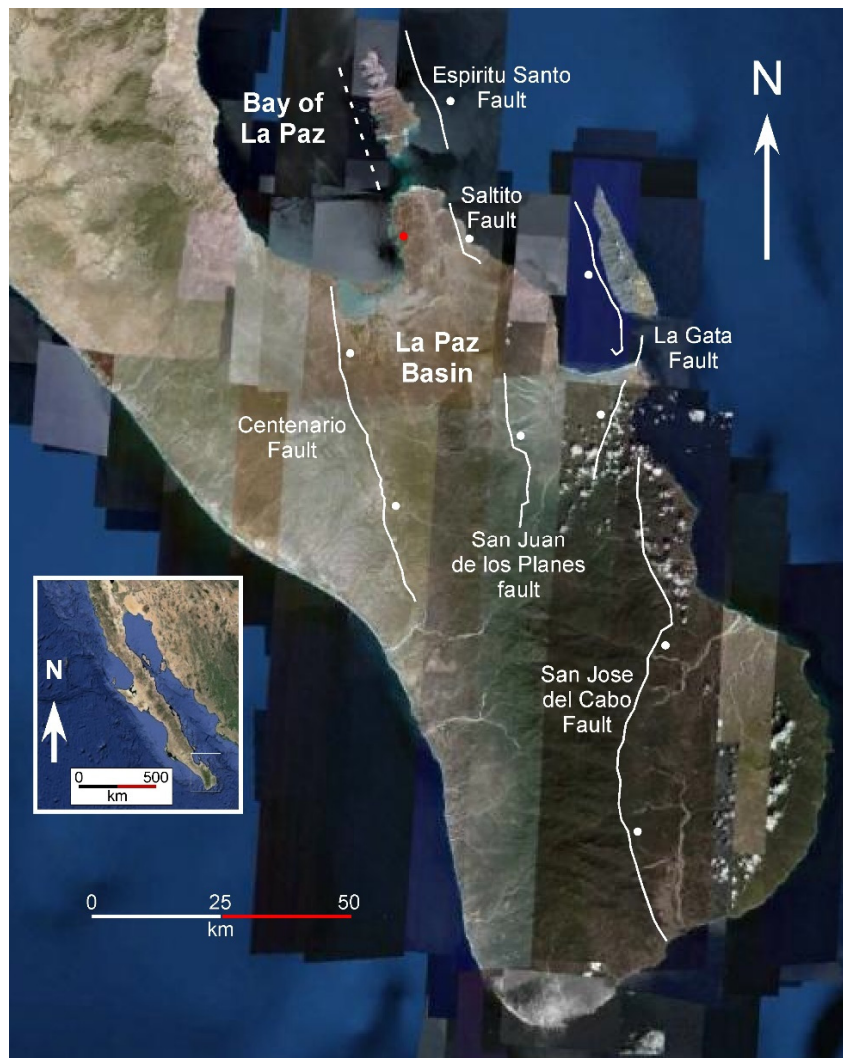


Figure 1. Location of study site. Major faults on the southern section of the Baja California peninsula, as described by Coyan and others [17], are displayed on Google Earth imagery, with dots marking the downthrown blocks. The dashed line represents an unnamed buried fault inferred by previous studies [21,22]. The red dot marks our study site. Inset displays the location of the Baja California Peninsula in relation to the Pacific coast of Mexico.

Detailed data for post-Wisconsin sea level changes are almost entirely lacking for the Pacific coast of Mexico. The single relevant curve, published in 1969 [23], shows a smooth rise of ~40 m to ~15 m below present sea level from 10,000 to 8000 BP, after which the rate of sea level rise steadily decreases, reaching ~1 m below present sea level by 3000 BP. There are no published records of relative sea level for the La Paz area.



Figure 2. Location of study site. Displayed on Google Earth imagery are (a); the Bay of La Paz, the city of La Paz, the Saltito Fault and the buried fault identified by [21,22] as occurring along the western flanks of the islands on the eastern edge of the bay. The area marked by the white square is expanded in (b); which displays the location of the two peninsulas surrounding Estero de Bahia Falso, our study site (white square) and the Pichilingue tidal gauge (red square). Estero de Bahia Falso is shown in greater detail in (c), with the location of core 4 marked by a white dot.

2.2. Bay of La Paz

Tides in the Bay of La Paz are mixed, mainly semi-diurnal [24], with a maximum tidal range of <2 m [25,26]. The bay is roughly oval with a maximum length of ~75 km N–S and 35 km E–W. The bay opens to the Gulf of California to the east, blocked in the south by several islands bounded on the west by an active fault [21,22], and a peninsula extending into the bay from the south (Figure 2a). The northern section of the bay is relatively deep, with a maximum depth of 420 m in the Alfonso Basin. Water depth in the southern third is <100 m [21,22,27,28]. Surface currents in the northern section are driven by a cyclonic gyre, especially in the fall, while currents are weak in the shallow southern third. Winds are seasonally variable, with weak (≤ 5 m/s) southwest winds prevailing during the summer winds, and stronger (≤ 12 m/s) northwest winds occur during the rest of the year [29], resulting in a water column that varies from weakly stratified in the winter to highly stratified in the summer [30]. The city of La Paz, the capital of the state of Baja California Sur, occupies the SW corner of the bay, <10 km from our site. The city has a population of >200,000 with an economy based largely on ecotourism and marine activities [31,32].

2.3. Study Site

Our study site is Estero de Bahia Falso, a lake located in a small bay tucked into the convoluted western edge of the southern peninsula, flanked by the 2.5 km long San Juan Nepomuceno (SJN) peninsula to the northwest, and the 1.25 km long Punta Colorado (PC) peninsula to the southeast (Figure 2b). The lake is in a small basin surrounded by steep, bare slopes rising to heights of >60 m. The lake is crescent-shaped, ~150 m \times 70 m in size, with a maximum depth of <1.0 m, and a surface elevation of ~1.25 m above mean high water (MHW). The lake drains an area of >1 km², with larger drainage systems to the northwest and the southeast constraining the catchment area to the immediate vicinity. Salinity was 49 parts per thousand (ppt) at the time of fieldwork in December 2011. The lake is fringed by a thin border of low halophytic shrubs, while red mangroves (*Rhizophora mangle*) form a denser, higher growth along the edge of the bay and black mangroves (*Avicennia germinans*) line the drainage channel that connects the lake to the sea near the lake's eastern end. The lake is separated from the sea by a low, flat ridge of shelly, sandy material which reaches a maximum elevation of ~75 cm above the lake level (~2 m above MHW). This ridge sits on top of a finer-grained beach that slopes to the sea. A salt pan surrounds the lake on the remaining three sides.

The site sits atop a thin alluvial Holocene fill on top of the Comondú Formation that consists of volcanic sandstones and conglomerates, rhyolitic ash-flows, tuffs and andesitic lahars and lava flows [11,31,33], above a Cretaceous basement of metamorphic and plutonic rocks [17]. The short (~2 km) normal north-dipping La Pedrera Fault occurs ~7 km to the northeast, beyond which the Cretaceous basement reaches the surface along the eastern side of the [31,33]. Movement along the Espiritu Santo Fault has resulted in a westward tilting and slow uplift of the peninsula [34]. Estimations of the rate of uplift vary. Calculations based on terrace deposits show a rate of 0.12–0.15 mm yr⁻¹ from the last interglacial, while data from an elevated platform suggests little or no uplift since that time. Calculations derived from the formation of notch suggest rates from 0.075 to 0.50 mm yr⁻¹ over the last 500–2000 years [34].

The long-term history of human use/disturbance of the area is unknown. However, until the recent development of a tourism-based economy human population levels were low, and the potential for anthropogenic disturbance slight. Material was moved for the construction of a roadway, which passes to the east of the lake, some of which has moved downhill. However the limit of this movement is clear and does not extend into our study areas.

3. Methods

This study focuses on the superficial sediments surrounding the lake, supplemented by data from core 4, taken from a site northeast of the lake's center, approximately 40 m behind the landward edge of the shell-covered beach ridge (Figure 2). The core was extracted from a water depth of ~0.6 m of water by means of a Russian peat borer in seven overlapping sections. All core sections were photographed and described in the field and hermetically sealed before being transported to the Global Change and Coastal Paleoecology Laboratory at Louisiana State University (Baton Rouge, LA, USA), where they were stored in a refrigerated room (4 °C). Surface samples were collected from the lake, the surrounding land surface and the subtidal nearshore area. Elevations and distances were determined by a Nikon range finder (Nikon Corporation, Toyko, Japan) with all locations marked by a hand held Garmin eTrex Venture global positioning system (GPS) unit. Although the listed accuracy of this unit is <15 m, this is the maximum error under poor satellite coverage. Field experience (reoccupying sites) has shown the practical uncertainty to be much less (<3 m). Photos were taken and sketches made of all relevant topographic and geological features. Shells and surface samples were collected from the terrestrial areas surrounding the lake. After opening in the lab, all core sections were photographed and physical properties described. Loss-on-ignition analysis was conducted continuously down the center of each section at 1 cm resolution. Small (~1 cc) samples were weighed wet, dried overnight at 100 °C, then weighed to determine water content (percentage of wet weight), following which they were burned at 550 °C for two hours and weighed to determine organic content (percent dry weight), and finally burned at 1000 °C for one hour and weighed to determine carbonate content (dry weight), following the procedure described by Liu and Fearn [35]. The precise alignment of core segments used to establish final core stratigraphy was based on the matching of the visual, compositional and elemental characteristics of the overlapping sediments. Elemental concentrations were determined by an Innov-X Delta Premium DP-4000 handheld X-ray fluorescence (XRF) unit for all surface samples and at 2 cm resolution down the length of the core (Olympus Corporation, Center Valley, PA, USA). The device analyzes each sample across three frequencies for 30 seconds per frequency producing elemental concentrations in parts per million (ppm) for the following elements: S, Cl, K, Ca, Ti, V, Cr, Mn, Fe, Co, Ni, Cu, Zn, As, Se, Br, Rb, Sr, Zr, Mo, Rh, Pd, Ag, Cd, Sn, Sb, Ba, Pt, Au, Hg, and Pb. We present data for K, Ti, V, Mn, Fe, Co, Zn, Br, and Mo, as representative terrestrial elements. The minimum and maximum error bars (in ppm) for each of these elements for the depth presented (0–35 cm) are: K: 75–140; Ti: 18–34; V: 21–34; Mn: 4–6; Fe: 58–112; Co: 17–26; Zn: 2; Br: 17–23; Rb: 1–2; and Mo: 1–3. The device was calibrated with certified standards NIST 2710a and 2711a.

Tidal amplitude is based on hourly data from a tide gauge located <5 km from our site at Bahia de Pichilingue for the period 15 May 1999 to 3 March 2011. 65,537 of the 103,464 possible hourly readings (63%) are recorded for this period. Due to the missing values we discarded data from months with less

than 240 readings (10 days), leaving a set of 95 months. The number of data points per month for the 95 months varied from 252 (once) to 744 (20 times).

Shells and shell fragments are ubiquitous on the shelly ridge fronting the ocean side of the lake, and also sparingly on the back side. Samples of some common types were collected and taken to the laboratory for identification and analysis. Given the immense number of shells encountered and the severely abraded nature of many, identification was performed only on randomly-selected shells, generally the best-preserved (Figure S1). No quantitative assessment of shell assemblages was performed. Shell identification was based on a regional book by Keen [36], plus the assistance of Dr. Emilio Garcia and the Louisiana Malacological Society. Similarly, coral fragments were simply listed as “coral”.

Radiocarbon dates were procured from five samples cut from marine shells and from a small subsample (~1 cc) of sediment extracted from a depth of 30 cm in core 4. The latter sample, which was selected in order to date a sedimentary change at the top of the core, was passed through a 63 micron sieve to remove silt and clay. Plant fragments were selected from the remaining material under a dissecting microscope after being washed in de-ionized water. This material was sent, along with the shell samples, to the National Ocean Sciences accelerator mass spectrometry (NOSAMS) laboratory at Woods Hole Oceanographic Institution (Woods Hole, MA, USA), where accelerator mass spectrometry (AMS) radiocarbon dating was performed by means of a 500 kV compact pelletron accelerator. The radiocarbon date for the plant material was calibrated to calendar years using Calib 7.0 and the INTCAL 13 curve, based on the dataset from Reimer and others [37]. The Calib 7.0 program provides a median probability date for each sample, calculated from the probability distribution. This value, which is considered a more reliable calibrated calendar date than the calibrated intercept date [38] is listed in the table and figures. Calibrated shell dates include a correction for the reservoir effect (old marine carbon) through the incorporation of the ΔR value of 253 ± 18 determined for the La Paz area by Frantz and others [39], and the MARINE13 curve.

Due to the extreme spatial heterogeneity of the material comprising the shelly ridge, sediment size was determined visually and reported qualitatively. Both the size of the sediments and the relative percentages of the different size categories (clay, silt, sand, gravel, boulders) varied so dramatically over short distances (both vertically and horizontally) (Figure S2) that quantitative analysis was not deemed as providing useful information.

4. Results

Unlike the uniformly fine-grained sediments of the salt pan which surrounds the eastern, western and northern edges of the lake, the sediments on the ocean side of the lake consist of a mix of material, highly variable both in composition and sediment size. Three areas of particular interest, marked A, B, and C, are highlighted in Figure 3.

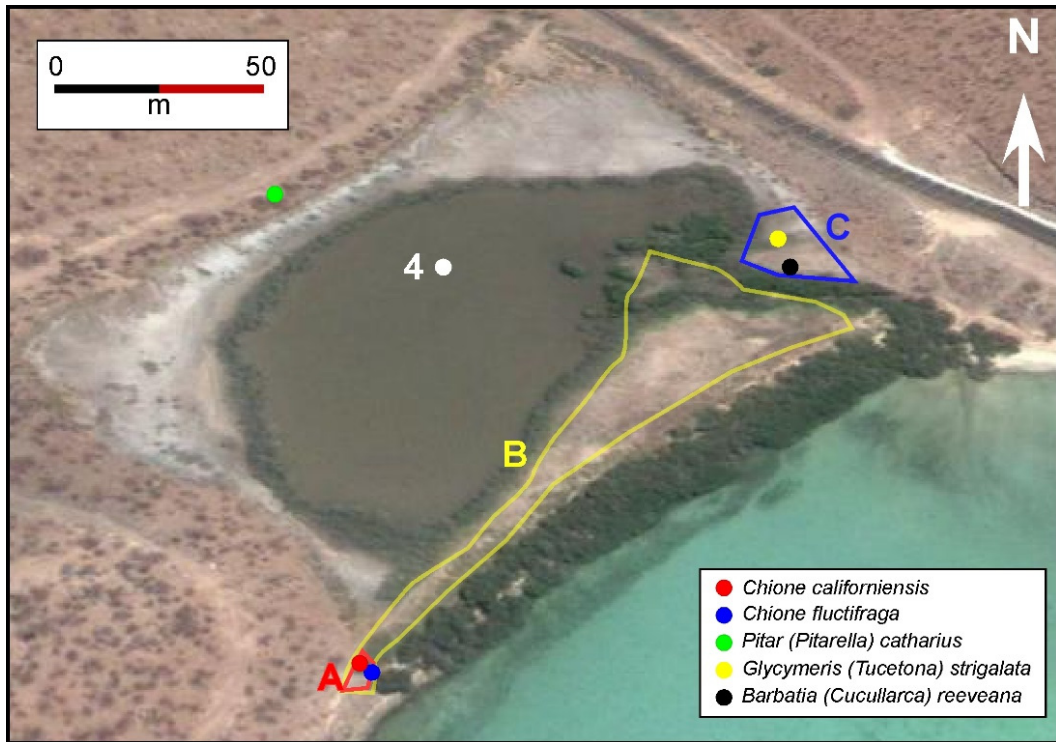


Figure 3. Marine deposits along the southern (seaward) edge of the lake. Three areas of interest are marked, as are the locations of the dated shells and core 4.

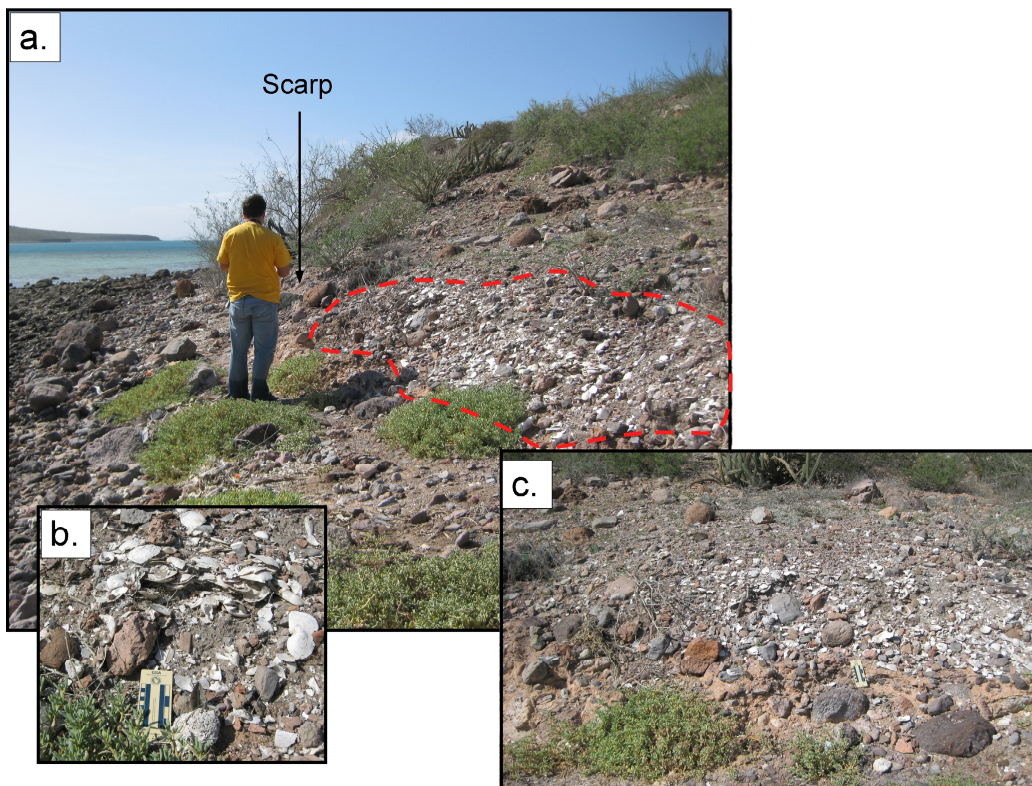


Figure 4. Area A. Area A is a small section of hillside (a) plastered with a shelly mixture of material, including angular boulders and imbricated shells (b); The layer sits above a reddish clay (c).

Area A is located at the western approach to the small basin that contains the lake. This area is notable for the veneer of mixed material covering a small section of the hillside located above and just landward of a steep (65°–70°) scarp (Figure 4). The sediments are a chaotic jumble of whole shells, disarticulated shells, shell hash and rocks embedded in a predominantly coarse sand matrix (Figure S3). In some sections the shells show evidence of imbrication (Figures 4b and S4). The shells represent species from a spectrum of marine environments. Examples include *Crassostrea* (oysters) that commonly occur in back bays, *Chione californiensis* and *Chionista fluctifraga* that inhabit intertidal and nearshore areas, offshore species, and coral fragments (Table 1, Figure 4). Shell preservation was inconsistent; degree of abrasion ranged from minimal (slight breakage on outside edges of shell, slight erosion of morphological features) to severe breakage. The rocks vary from rounded to extremely angular, indicating large differences in the distance and duration of transport. While the rounded rocks likely originated from the sea, the degree of angularity suggests a terrestrial provenance for some. Sediment varies in size from mud through silt, sand, gravel, cobble, and boulders. The area covered by this mixture is spatially constrained, both laterally and vertically. Maximum lateral extent is ~10 m (~half is shown in Figure 4a), while the vertical extent of the massive shell coverage is ~1.5 m, covering the hillside from ~0.5 m to 2 m above MHW. Less densely packed shells extend the vertical range an additional ~0.5 m upwards. This layer sits above a layer of orange clay (Figure 4c).

Table 1. Name, geographic range and radiocarbon and calibrated dates for identified shells.

Shell Information			Dating Results			
Genus (Subgenus) Species	Geographic Range (Depth)	Lab #	¹⁴ C Age	Error	2σ Range	Median Probability (Year BP)
<i>Pitar (Pitarella) catharius</i>	West coast of Baja California to Gulf of California (13–80 m)	OS-110978	2020	20	1259–1374	1311
<i>Chione (Chione) californiensis</i>	California to Panama (intertidal to 69 m)	OS-110979	2180	20	1387–1549	1475
<i>Chione (Chionista) fluctifraga</i>	California, Gulf of California, Sonora (intertidal)	OS-110980	2340	25	1560–1765	1660
<i>Glycymeris (Tucetona) strigilata</i>	Gulf of California to Ecuador (13–110 m)	OS-110981	1740	20	951–1130	1032
<i>Barbatia (Cucullaearca) reeveana</i>	Gulf of California to Peru (intertidal to 120 m)	OS-110982	2310	20	1540–1706	1627
<i>Spondylus princeps</i>	Gulf of California, Pacific coast from Baja California Sur to Peru (15–50 m)	NA	NA	NA	NA	NA

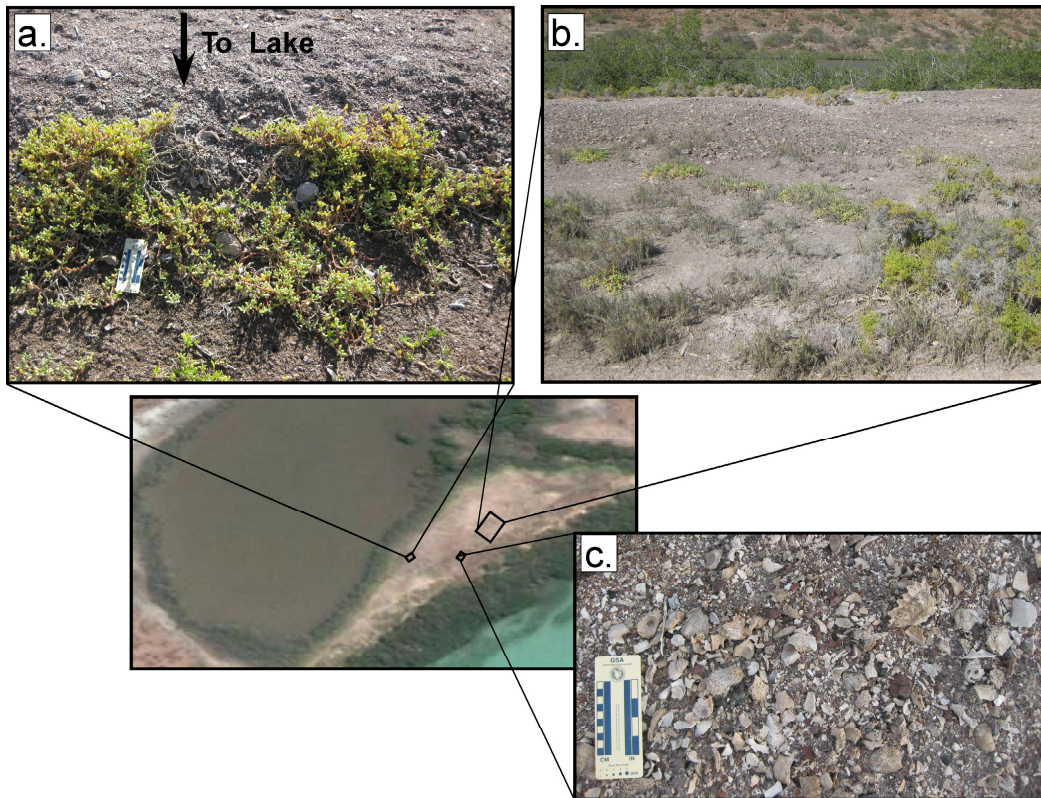


Figure 5. Area B. Area B consists of a wedge–shape deposit with a maximum thickness of ~50 cm, consisting of an extremely poorly-sorted mix of marine and terrestrial material. Size varies, although the largest boulders are absent. Clear cliff faces occur on both the seaward and landward edges.

There is no apparent sorting, with sediment size exhibiting extreme spatial heterogeneity over very small distances (Figure S2). Boulder-sized rocks are rare or absent (Figure 5c). This ridge reaches a maximum thickness of ~50 cm and sits incongruously on top of a fine-grained surface that slopes down to the bay. The ridge exhibits cliff faces on both the lake and ocean sides (Figure 5a,b). As with the material in Area A, shell preservation was highly variable and identifiable shells represent a variety of marine environments. The top of the ridge is ~2 m above MHW.

Loss-on-ignition analysis indicates that on average the ridge sediments (4.8%) were nearly twice as organic as either the beach (2.9%) or nearshore samples (2.5%), while containing less than half as much carbonate material (11.9%) as either the beach (32.2%) or nearshore samples (26.0%). Elemental concentration values for ridge samples are intermediate between the marine (offshore and beach) and terrestrial (hillslopes) samples for both terrestrial (Ti, V, Mn, Fe, Zn) and marine (Ca, Sr) elements (Figure S5).

Area B, which extends along the entire front of the lake, is basically a low shelly ridge composed of a mixture of mainly marine sediments. Like the mixture in Area A, the sediments consist of a sand matrix containing a jumble of shells, shell and coral fragments, and rocks, both rounded and angular.

Area C is at the extreme eastern edge of the lake, at the base of a steep (~45°) hillside rising to a height of ~60 m. As in the other two areas, the materials in this location consist of a mixture of shells, shell and coral fragments, and rocks in a sandy matrix (Figure 6). Shells found here include *Glycymeris (Tucentona) strigilata*, whose preferred habitats range from 13 to 110 m [38]. The sediments

form a distinct pile, with a sharp cliff face on the northern edge, with a maximum thickness of ~60 cm (Figure 6A). These sediments, marked by a sharp contact, sit on top of a relatively flat surface of fine-grained sediments.

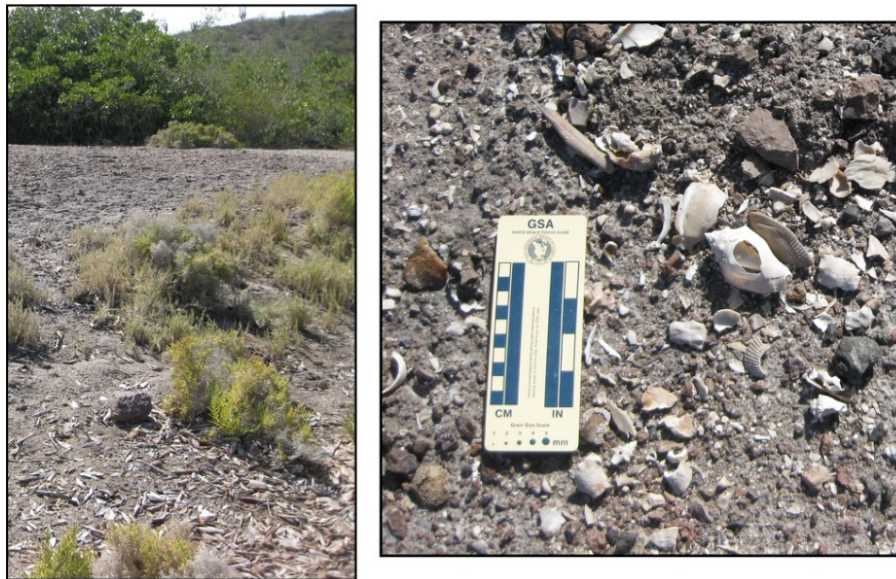


Figure 6. Area C. Area C is a mound of mixed materials, formed at the eastern edge of the lake at the base of a steep slope; thickness is ~60 cm.

Core Stratigraphy

The top of core 4 displays a dramatic stratigraphic change (Figure 7). The top 27 cm consist of a low-organic (6%–10%) brown clay. At 28 cm organic and water contents jump from 9% to 33% and from 47% to 74%, respectively. This marks the stratigraphic change to peat, which dominates the core down to a depth of, ~260 cm (core photo, far left, and the loss-on-ignition graph, center left, Figure 7). The transition at 27 cm (photo, middle) is not only abrupt; it is also marked by irregular deposition with clasts from the underlying peat embedded in the more clastic material (white dashed circle). The geochemical profile also changes at this transition, with the material above 27 cm having distinctly higher concentrations of K, Ti, Mn, Fe, Co, Zn, Rb, and Zr and lower concentrations of Mo and Br than the underlying peat (right), matching the profiles of samples taken from the surrounding hillsides. The plant fragments sampled at 30 cm were dated to 1170 ± 20 ¹⁴C year BP, which calibrates to a median date of 1106 cal year BP (Table 2).

Table 2. Radiocarbon and calibrated dates of sediment sample from Core 4.

Name	Type	Lab #	¹⁴ C Age	Error	2σ Range	Relative Probability	Median Probability (Year BP)
CRE 4A 30 cm	Plant/Wood	OS-111567	1170	20	1007–1024	0.07	
					1053–1176	0.93	1106

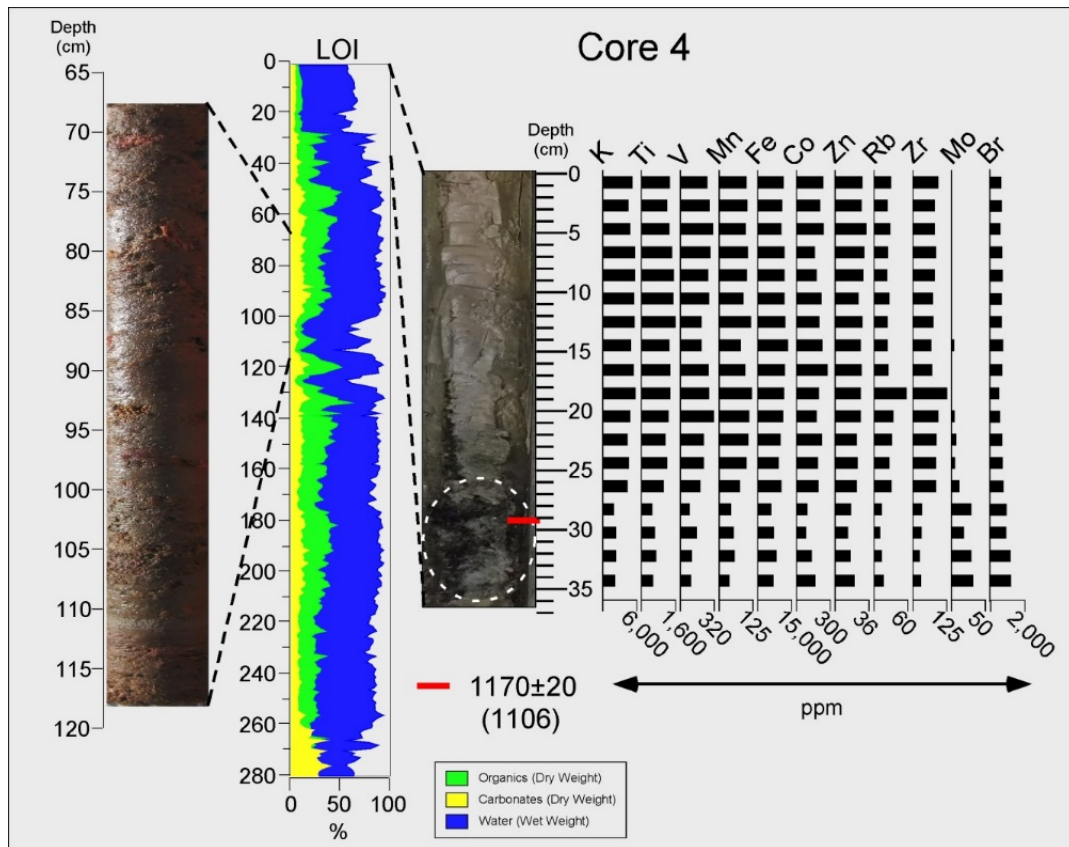


Figure 7. Sediment core 4 from near the center of the lake. Above a calcareous bottom mud from 281 to 262 cm (LOI diagram, center left), the core is predominately organic as shown by the section from 67 to 117 cm (left). Above a boundary at 27 cm, marked by the presence of encapsulated clasts from the underlying material (center right), the sediments abruptly change to a lacustrine mud with an altered geochemical signature (right). The red line marks the depth of the dated sample which returned a median calibrated date of 1106 year BP.

5. Discussion

Areas A, B, and C all contain a mélange of divergent material. Marine elements include shells and corals from the intertidal to deeper offshore water, with the published vertical range of three of the identified shell species beginning at a minimum depth of 13 m (Table 1). The size, angularity, and physical appearance of some rocks occurring within this mélange suggest that the material was derived at least partially from the surrounding hillsides. This is supported by both the geochemical and compositional profiles of the ridge samples, which have elemental concentrations intermediate between the marine and terrestrial samples, and higher organic and lower carbonate percentages than the marine samples (Figure S5).

Changes in either eustatic or relative sea level can potentially explain the presence of this material as being deposited on a beach during a period of higher water. There is no evidence for a former highstand as the single sea level curve for the area [23] indicates that eustatic sea level was never higher than the present. Recent compilations of uplift-corrected Holocene records from farther north show very similar eustatic records, notably lacking any highstands [40,41].

Relative sea level change is a more likely possibility, given the active tectonic nature of the region. Again, concrete evidence is lacking, as there appears to be no published data concerning seismically-driven vertical motion for the area. In general geologic terms, sudden upward movement at the site does not seem highly likely. The site is situated within the upper edge of the La Paz basin, which being a half graben, is prone to downward movement. The faults in the areas are mainly east-dipping normal faults with vertical motion dominated by downward movement of the hanging walls [17]. Two small faults occur in the vicinity of the study site. Neither is mentioned in a recent, detailed study of the area's faults [17], presumably due to their relative insignificance. The effects of the nearest, the west-dipping Balandra Fault, if felt, would likely result in depression, rather than uplift at the site [33]. The shorter, more distant north-dipping La Pedrera Fault is less likely to result in upward movement at Estero de Bahia Falso. The evidence, derived from studies of adjacent sea notches, for continuing slow uplift suggests that sudden vertical movement has not occurred over the period of notch formation, estimated to have covered the last 500–2000 years [34]. The uplift rates, derived from three different proxies, vary from 0.0 to 0.5 mm year⁻¹, producing estimated vertical movement from 0 to 50 cm per 1000 years. The ability of this movement to explain the material in Areas A, B, and C as uplifted marine sediments depends, of course, on the age of the material. This is discussed below.

However, although sudden, seismically-generated vertical movement at the site cannot be definitively eliminated, and slow uplift has likely occurred, internal evidence suggests that if either process resulted in changes in relative sea level, such changes were not sufficient to be responsible for the deposition of the anomalous sediments. With the surface of the lake ~75 cm below the top of the shelly ridge, the 60 cm water depth puts the top of core 4 about 135 cm below the top of the ridge. If the ridge represents approximate sea level at some earlier period the expected sedimentation at core 4, under >1 m of water at the time, would likely be marine clays, not peat. Similarly it seems unlikely that a beach ridge resulting from higher sea level would contain organisms from such a wide range of marine environments.

Another possibility is that the ridge formed as a beach under normal coastal processes and then was abandoned in its present location as the beach prograded seaward. Gradual progradation is, indeed, the process that most likely built the underlying beach, which is a smooth, low-gradient surface composed of well-sorted, uniformly-sized, rounded, fine-grained sediments. All of these features are characteristic of gradual deposition in low-energy environments. However, the shelly ridge sitting on top of this material has distinctly different physical properties. The material is extremely poorly sorted and extremely heterogeneous, both spatially and compositionally, containing, as it does, biological material from across a spectrum of marine environments. The geochemical and loss-on-ignition profiles suggest a significant terrestrial contribution to the material, as does the angularity of many of the larger clastic elements. These characteristics strongly suggest that this ridge did not form under low-energy conditions.

The ridge's formation as part of a chenier plain, which usually forms as a result of shifting sediment supplies and the winnowing of shelly material from the underlying mud flats, seems unlikely. The presence of angular rocks, broken corals, and offshore shell species does not agree with this formation process, nor is there any reason to suggest long-term shifts in either sediment supply or wave energy in this small, protected bay.

The same arguments can be applied to Area A, which contains material from a similar mix of marine environments. Additional arguments against Area A as an uplifted marine environment include the composition of the underlying sediments and the spatial extent of Area A. The clean, shell-free,

boulder-embedded orange clay occurring directly below the shell layer (Figure 4C) closely resembles the surrounding hillsides. If the Area A shell layer represents an uplifted sea bed, the underlying material should also be marine. It is difficult to imagine a scenario in which a section of seafloor as small as Area A (~10 m × 1.5 m) could be uplifted and emplaced within an area surrounded by terrestrial environments both vertically and horizontally. Positing that Area A and Area B result from a period of higher relative sea level poses an additional problem in that Area A, representing the sea floor, is at slightly higher elevation than Area B, representing the contemporaneous beach.

Because deposition under normal, fair weather conditions under the current environmental setting does not explain the presence of this material, and neither changes in relative sea level nor vertical movement seem likely, some type of high-energy event becomes the most likely possibility. The piled material in both Area B and Area C is of generally marine origin, and has been deposited as a coherent, spatially continuous unit on top of a distinctly different (and finer-grained) surface, with obvious cliff faces. Identification of this as an event deposit seems the most reasonable.

Evidence from the sediment core suggests that the wetland deepened as a result of the deposition of this event deposit. The upper 27 cm of core 4 consist of a fine dark, low-organic mud with geochemical properties associated with runoff from the surrounding slopes, *i.e.*, a sediment type commonly found on the bottom of shallow coastal lakes in non-carbonate environments. However, apart from a clastic interval (~100–130 cm in core 4), the underlying material, to a depth of ~260 cm is peat. Prior to the transition to lake the area appeared to have been a vegetated wetland of fluctuating water depth, probably in a shallow depression behind a low seaward sill that retarded drainage to the sea. The depositional transition to lake mud indicates a deepening of the flooded wetlands into an open-water lake. This transition, dated to ~1100 year BP in core 4, is marked by turbulent deposition, suggesting a high-energy event.

The physical characteristics of the sedimentary unit covering the small section of hillslope in Area A suggest that this material was deposited under high-energy conditions. The elevation of the site, the presence of coral fragments and deep water marine shells, their imbrication and abraded nature all indicate transport during high water under turbulent conditions.

Occasional shells occur on the hillslopes to the north of the lake, including a *Pitar* (*Pitarrella*) *catharius* shell, an offshore species with a depth range from 13 to 80 m [36]. *Glymeris* (*Tucetona*) *strigilata* is another identified offshore species, occupying a similar depth range. Of particular interest is the presence of the upper valve of a *Spondylus princeps* (Pacific thorny oyster), a bivalve species that lives at depths of 15 to 50 m [42] from the Gulf of California and the Pacific coast from Baja California Sur to Peru [43]. *Spondylus* is much more firmly attached to the bottom than other bivalves, typically cementing itself to a solid substrate rather than attaching by byssus threads [44]. This oyster species is also noted for the strength of its ball and socket valve hinge, which is much stronger than the toothed hinge common to other bivalve molluscs. If living at the time of transport, an extremely turbulent force, such as occurs only during a tsunami or intense storm, would have been required to dislodge the upper valve from the firmly-cemented lower valve and transport it from an offshore depth to our study site.

Between the seaward edge of the shelly ridge (Area B) and the bay the ground slopes smoothly, dropping ~1.50 m from the base of the ridge, traversing a barren area of fine-grained material before encountering the landward edge of the mangrove fringe. The surface of the beach and the ground beneath the mangroves are littered with such floatable debris as empty soft drink bottles and styrofoam containers. The line of maximum landward deposition of these objects, presumably corresponding to the

reach of the maximum wave height under ordinary conditions (including recent tropical cyclones) is just landward of the mangroves, ~50 cm below the top of the ridge. This supports the view that the event responsible for transporting the materials associated with Areas A, B, and C generated extremely high water levels and/or wave energy. Similar conclusions result from the presence of coral and deep-water shells and the occurrence of rocks apparently transported from the surrounding hillsides. The elevation of both the massive shell coverage in Area A and the top of the ridge in Area B are ~2 m above MHW.

The event most likely occurred around 1100 year BP, although the exact age is somewhat uncertain. Calibrated dates for shells associated with the event range from 1706 year BP to 951 year BP. A wide range in ages is expected as many of the transported shells may have been lying on the sea bottom for centuries before being entrained. However these shells do provide a maximum age of 1130 year BP, the oldest possible date for the youngest dated shell. This is in rough agreement with the sample from the sediment core, with calibrated dates that range from 1176 to 1007 year BP, with a median probability of 1106 year BP. Because the estimated rates of slow uplift can only account for maximum vertical movement of 50 cm over the last 1000 years, this uplift cannot be responsible for the placement of the marine sediments at their present elevations.

Average monthly tidal difference for the 95 months examined was 164 cm. We consider this a conservative estimate of tidal range as data from some months was partial, thereby possibly reducing maximum amplitude due to the missing of the monthly extremes. The range of monthly amplitude varied from 191 cm (January 2006) to 114 cm (March 2000, for which only 11 days of data were recorded). Tide gauge data shows a range of >2 m for the period from 15 May 1999 to 3 March 2011 (Figure 8).

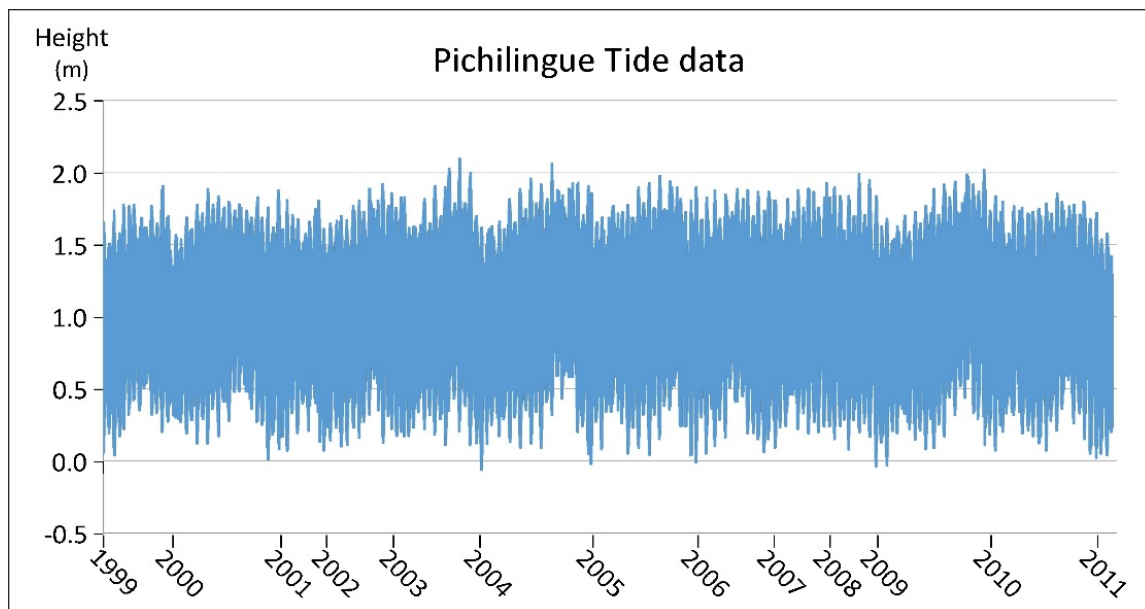


Figure 8. Tide heights at Pichilingue gauge station for the period 15 May 1999 to 3 March 2011.

A tidal amplitude of 1.64 m equates to potential elevation range of ~2–3.6 m above water level for the marine deposits at the time of the event. This should be considered the minimum potential run-up due to the conservative tidal range estimation; in addition, the presence of scattered shells at higher elevations and occasional occurrence on slopes to the north of the lake suggests that the maximum water depth might have been greater.

5.1. Extreme Events

High-energy events for the area are limited to tsunamis and tropical cyclones. Hurricanes are fairly frequent in the area, with 10 hurricanes having passed within 50 km of La Paz since 1949, the beginning of the instrumental record (Figure 9) [45], including two category 3 hurricanes, one category 2 hurricane, and seven category 1 hurricanes. Extending the radius to 100 km produces another six hurricanes, all category 1. In the eastern North Pacific, the El Niño-Southern Oscillation (ENSO) exerts an important control over tropical cyclones, as over the instrumental period, tropical cyclones have been more frequent [46–48], and more intense [49,50] during El Niño than neutral and La Niña periods for the region.

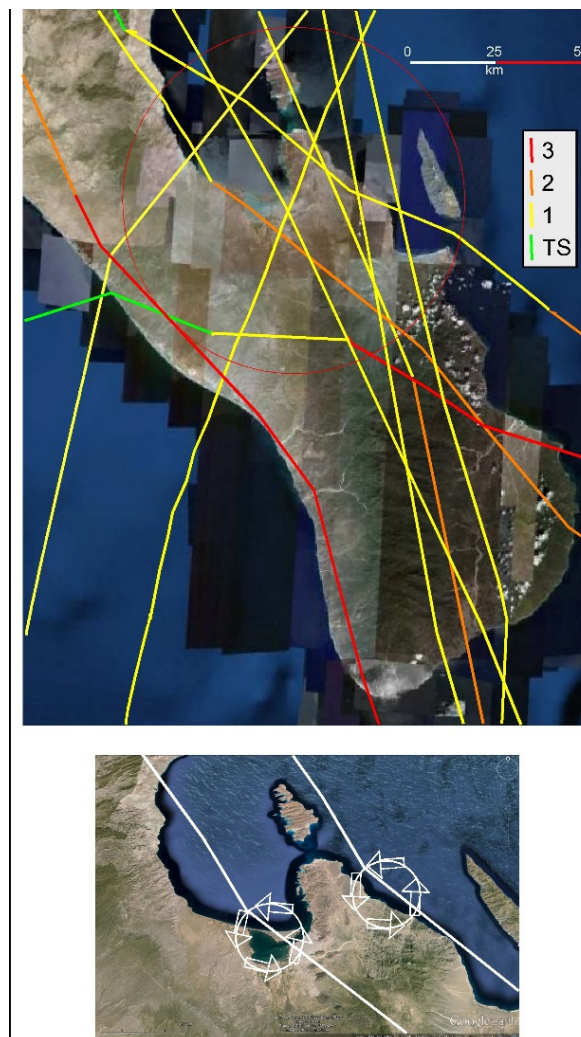


Figure 9. Hurricane history for the La Paz area. Displayed are the tracks of all tropical cyclones that approached within a 50 km radius (red circle) of the city of La Paz at hurricane strength from 1949 to 2014 (top). Five of the ten storms passed to the east of our site, much of their force blocked by the protruding peninsula along the southeastern edge of the bay. Cartoon at bottom shows the cyclonic circulation of hypothetical tropical cyclones with arrows pointing in the direction of wind flow for all four quadrants, demonstrating that storms passing to the west will generally result in an off- shore direction for wind/wave energy, and consequently sediment transport during the passage of the strong right front quadrant. Force of storms passing to the east will be dampened by the intervening peninsula.

The sedimentary signatures of both tsunami [51–57] and tropical cyclone-generated [58–66] deposits have been extensively studied. However, attempts at distinguishing between the two [51,53,55,67] have not been entirely successful. This is due not only to the large overlap of sedimentary features common to both tsunami and tropical cyclone-generated deposits, but also to the highly idiosyncratic depositional patterns of individual events, driven by differences in such parameters as coastal geomorphology, bathymetry, topography, and size and direction of travel [68].

Under current conditions, the deposition at Estero de Bahia Falso seems unlikely to have been generated by tropical cyclones, given the relatively weak tropical cyclones that have impacted the area during the instrumental period (Figure 9), as it is doubtful that storms of this magnitude could generate the surge and wave energy capable of either transporting the large cobbles as far inland as Area C (Figure 6b) as suspended sediment; or depositing the mud/silt/sand/cobbles mixture as bedload.

However, paleorecords show a large increase in ENSO activity for Ecuador [69] starting ~1500 BP and for the Alfonso Basin [70] at ~1000 BP, perhaps corresponding to more frequent and more powerful tropical cyclones near our site during that period. Although paleoclimatic conditions increase the possibility of the passage of an exceptionally powerful tropical cyclone ~1000 years ago, geographical parameters tend to dampen the wave energy of tropical cyclones at the site for two reasons. First, the small fetch acts to limit extreme wave heights, although some potential funneling of wave energy due to coastal morphology is possible under specific wave and wind conditions. Secondly, tropical cyclones, which typically track from south to north in this region, will rarely generate strong onshore winds at the site. Storms passing to the east will result in offshore winds coming from the north and east, from which the lake is well protected by the bulk of the intervening peninsula to the east, which is marked by a rocky spine with elevations >430 m [71]. For storms passing to the west, the lake is subjected to offshore winds and waves during the passage of the strong right front quadrant. It is only after the eye of the storm has passed, during the passage of the weaker right rear quadrant, that the site will be subjected to onshore winds (Figure 9). Furthermore, the intensity of such storms will generally have already been reduced by their transit across the dry peninsula to the south. Additionally, sorting, which is perhaps the characteristic most likely to differentiate tsunami and storm deposits, is extremely poor for the deposits in all areas, especially in Area A where boulders >50 cm in length are mixed with mud, silt, and sand.

The constricted spatial extent of the event deposit, especially the absence of the shelly material along the seaward edge of the beach plain in Area B, is more consistent with the spread of a single, focused surge of water moving up-channel upon reaching the open embayment than with the persistent landward force of waves occurring over the duration of a tropical cyclone. However, this is not a definitive distinguishing feature, as evidenced by the extremely short periods (0.5–1 h) of peak flooding documented for the fast moving Typhoon Haiyan in 2013 [72]. Although a tropical cyclone cannot be eliminated as a candidate process, it would likely have required an unusually large and/or intense storm on a fortuitously-positioned track to generate sufficient energy to transport the anomalous marine material found in Areas A–C.

5.2. Tsunamis

The most likely candidate is a tsunami. Given the protection offered by the Baja California Peninsula, tele-tsunamis from the open Pacific likewise are an unlikely source of such a high-energy event. Large

earthquakes occur along the axis of the plate boundary in the central Gulf of California [21,22,73], creating the potential for tsunamis, although the strike/slip nature of the boundary tends to limit vertical movement. However, our study site is protected to a large degree from the effects of such tsunamis by the configuration of the Bay of La Paz, with the eastern islands blocking the entrance to the bay, and especially by the protruding southern peninsula on which our study site is located. These islands are aligned on faults along their western edges, which have been the epicenters of numerous earthquakes throughout the historic period [22], as evidenced by multiple large turbidite layers recorded from the floor of the Alfonso Basin in the northern section of the Bay of La Paz [21,22]. These turbidite layers have been attributed to large, seismically-induced slope failures on the western edges of these islands. The estimated basin-floor volume of the largest turbidite, which is up to 80 cm thick at >10 km offshore, is 10^8 m^3 . Not only is this 3–4 orders of magnitude larger than the volume of turbidites associated with tropical cyclones in the same record [22], it is also larger than the total estimated volume ($30 \times 10^6 \text{ m}^3$) of the rockslide that produced the 524 m high 1958 tsunami in Lituya Bay, Alaska [6].

It seems reasonable that such slumps could produce large local tsunamis, particularly in the shallow southern section of the bay. Wave focusing resulting from the site's location at the end of a blind bay enclosed within the km-long arms of peninsulas to both the north and south could further increase wave height and energy [74].

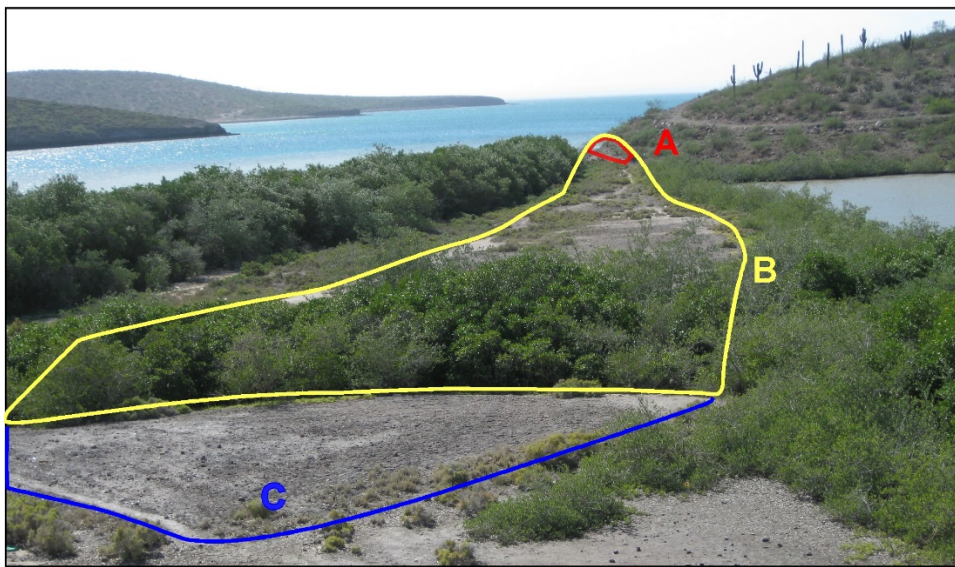


Figure 10. Topography and orientation of the deposited marine material. Looking westward down the inferred path of the marine intrusion. Area A (red) where the largest material was plastered against the hillside is located at the lowest elevation nearest the bay. Mixed sediments, minus the largest terrestrial boulders spread laterally across Areas B (yellow) and C (blue). Steep cliff faces on both sides of the shelly ridge in Area B suggest a narrow path for the wave energy, perhaps due to the angle of approach and the geometry of the projecting hillside. The extension of the reverse of this line leads down the center of the subbay, and eventually towards the city of La Paz.

Such an event would explain the unique geological/geomorphological features observed at the site. When viewed from the eastern end of the lake, the history of the inferred tsunami can be visualized

(Figure 10). Area A is located at the closest approach to the lake from the open bay, immediately inside the last projecting hillside. It is likely that the tsunami wave, carrying a load of marine sediments, including corals and shells, living and dead, from a variety of depths, hit the edge of the protruding hillside, scarping the corner and entraining the surface boulders, before slamming into Area A, imbricating shells and plastering the mixed material into the existing hillside. Constrained by the angle of impact the tsunami would have then spread out over the flat terrain (Area B), depositing the thick carpet of material over the foreshore before smashing against the steep hill at the eastern end of the embayment and dropping the entrained sediments (Area C). The ridge of newly deposited material would likely have impounded the marine water, transforming the wetland into a body of open water. Area B and Area C, visually part of the same depositional feature, would, at some point, have been bifurcated by the drainage channel from the lake. This channel, which cuts through the shelly ridge in Area B, might have formed either during the event due to the force of the tsunami back flow, or at a later date during periods of increased precipitation and increased stress on the barrier. The surrounding salt pans, indications of a larger lake, may be related to either the original impoundment or to later variability in precipitation/evaporation levels.

5.3. Local Event History

Gonzalez-Yajimovich and others [22] document three large turbidites over the last 4900 years, the last occurring at ~1500 year BP, all of which they attribute to slumping of the eastern islands. It is possible that the ~1100 year BP event documented at our site corresponds to the 1500 year BP event inferred from the turbidite record. However, it is also possible that our event does not match any major event in the turbidite record, perhaps indicating that even relatively small events can result in tsunamis >2 m in height with devastating impacts at some localities along the Bay of La Paz. This is a risk that needs to be incorporated into local vulnerability studies.

Further research should help to confirm a tsunami as the proximate cause of these anomalous sediments. Examinations of adjacent sites should provide supporting evidence for the occurrence of this event and help determine its spatial extent, while the identification and statistical analyses of a larger number of shells and coral fragments, both at the site and offshore, may produce useful information regarding the path of the wave.

6. Conclusions

Anomalous, mainly allochthonous sediments occur seaward of Estero de Bahía Falso, a shallow lake occupying a small embayment along the western edge of the peninsula extending into the southeastern section of the Bay of La Paz, in Baja California Sur, Mexico. The sediments consist of a mixture of marine and terrestrial material, including biogenic marine material from a wide range of marine environments and depths, including shells of three species with depth ranges >13 m. The material is plastered against the hillside at the western opening of the embayment, beyond which the sediment cover widens and flattens eastward, culminating in a thick, structureless deposit at the base of a steep hillside at the eastern end of the embayment. The deposition of this material coincides both chronologically and stratigraphically with a higher water level within the area occupied by the current lake. We interpret

these features as most likely resulting from an extreme wave event with a minimum runup of ~2–3.6 m above MHW, which we suggest can be attributed to a paleotsunami occurring ~1100 year BP.

This probable tsunami was likely generated by the seismically-induced slumping of the western edge of one or more of the islands along the eastern edge of the bay. Because such events, which Gonzalez-Yajimovich and others [22] suggest have occurred repeatedly in the past, are associated with an active fault, they are likely to reoccur in the future. Such events present a significant societal risk to the nearby city of La Paz, a metropolitan area with marine tourism-based economy [31,32]. Therefore, we suggest that the potential for devastating tsunamis generated by relatively small events in enclosed waters is a geological risk that needs to be fully incorporated into coastal vulnerability studies. This applies specifically to La Paz, but also more broadly to other tectonically-active areas with steep topography surrounding confined bodies of water.

Acknowledgments

Funding was provided by IAI grant SPG-CRA-2050 to Kam-biu Liu. We wish to thank Luis Farfan (CICESE) and Graciela Raga (UNAM) for logistical support and Emilio Garcia for his help in identifying shells.

Author Contributions

K.-B.L., T.A.M., and T.A.B. conceived and conducted the fieldwork involved in this project. T.A.B. and T.A.M. conducted the laboratory analysis along with K.-B.L. T.A.M. primarily wrote the article which was edited and revised by T.A.B. and K.-B.L.

Conflicts of Interest

The authors declare no conflict of interest.

References

1. Lay, T.; Kanamori, H.; Ammon, C.J.; Nettles, M.; Ward, S.N.; Aster, R.C.; Beck, S.L.; Bilek, S.L.; Brudzinski, M.R.; Butler, R.; *et al.* The Great Sumatra-Andaman Earthquake of 26 December 2004. *Science* **2005**, *308*, 1127–1133.
2. Paris, R.; Lavigne, F.; Wassmer, P.; Sartohadi, J. Coastal sedimentation associated with the December 26, 2004 tsunami in Lhok Nga, west Banda Aceh (Sumatra, Indonesia). *Mar. Geol.* **2007**, *238*, 93–106.
3. Fujii, Y.; Satake, K.; Sakai, S.; Shinohara, M.; Kanazawa, T. Tsunami source of the 2011 off the Pacific coast of Tohoku Earthquake. *Earth Planets Space* **2011**, *63*, 815–820.
4. Mori, N.; Takahashi, T.; Yasuda, T.; Yanagisawa, H. Survey of 2011 Tohoku earthquake tsunami inundation and run-up. *Geophys. Res. Lett.* **2011**, *38*, L00G14.
5. Heidarzadeh, M.; Satake, K. Waveform and spectral analyses of the 2011 Japan tsunami records on tide gauge and DART stations across the Pacific Ocean. *Pure Appl. Geophys.* **2013**, *170*, 1275–1293.
6. Weiss, R.; Fritz, H.M.; Wünnemann, K. Hybrid modeling of the mega-tsunami runup in Lituya Bay after half a century. *Geophys. Res. Lett.* **2009**, *36*, L09602.

7. Miller, D.J. *Giant Waves in Lituya Bay, Alaska*; USGS Professional Paper 354-C; United States Government Printing Office: Washington, DC, USA, 1960.
8. Voight, B.; Janda, R.J.; Glicken, H.; Douglass, P.M. Nature and mechanics of the Mount St Helens rockslide-avalanche of 18 May 1980. *Géotechnique* **1983**, *33*, 243–273.
9. Müller-Salzburg, L. The Vajont catastrophe-A personal review. *Eng. Geol.* **1987**, *24*, 423–444.
10. Müller-Salzburg, L. The rock slide in the Vajont Valley. *Rock Mech. Eng. Geol.* **1964**, *2*, 148–212.
11. Hausback, B.P. Cenozoic volcanic and tectonic evolution of Baja California Sur, Mexico. In *Geology of the Baja California Peninsula*; Pacific Section Special Paper 39; Frizzell, V.A., Jr., Ed.; Society of Economic Paleontologists and Mineralogists: Tulsa, OK, USA, 1984; pp. 219–236.
12. Atwater, T. Implications of plate tectonics for the Cenozoic tectonics of western North America. *Geol. Soc. Am. Bull.* **1970**, *81*, 125–133.
13. Stock, J.M.; Hodges, K.V. Pre-Pliocene extension around the Gulf of California and the transfer of Baja California to the Pacific Plate. *Tectonics* **1989**, *8*, 99–115.
14. Mayer, L.; Vincent, K.R. Active tectonics of the Loreto area, Baja California Sur, Mexico. *Geomorphology* **1999**, *27*, 243–255.
15. Sumy, D.F.; Gaherty, J.B.; Kim, W.-Y.; Diehl, T.; Collins, J.A. The mechanisms of earthquakes and faulting in the southern Gulf of Mexico. *Bull. Seismol. Soc. Am.* **2013**, *103*, 487–506.
16. Fletcher, J.M.; Kohn, B.P.; Foster, D.A.; Gleadow, J.W. Heterogeneous Neogene cooling and exhumation of the Los Cabos block, southern Baja California: Evidence from fission-track thermochronology. *Geology* **2000**, *28*, 107–110.
17. Coyan, M.M.; Arrowsmith, J.R.; Umhoefer, P.; Coyan, J.; Kent, G.; Martínez Gutiérrez, G.; Driscoll, N. Geometry and Quaternary slip behavior of the San Juan de los Planes and Saltito fault zones, Baja California Sur, Mexico: Characterization of rift-normal faults. *Geosphere* **2013**, *9*, 426–443.
18. Ortlieb, L. Quaternary shorelines along the northeastern Gulf of California: Geochronological data and neotectonic implications. In *Studies of Sonoran Geology*; Special Paper 254; Pérez-Segura, E., Jacques-Ayala, C., Eds.; Geological Society of America: Boulder, CO, USA, 1991; pp. 95–120.
19. Ortlieb, L. Quaternary vertical movements along the coasts of Baja California and Sonora. In *The Gulf and Peninsular Province of the Californias*; Dauphin, J.P., Simoneit, B.R.T., Eds.; American Association of Petroleum Geologists: Tulsa, OK, USA, 1991; Memoir 47, pp. 447–480.
20. Welles, D.L.; Coppersmith, K.J. New empirical relationships among the magnitude, rupture length, rupture width, rupture area, and surface displacement. *Bull. Seismol. Soc. Am.* **1994**, *84*, 974–1002.
21. Gorsline, D.S.; de Diego, T.; Nava-Sanchez, E.H. Seismically triggered turbidites in small margin basins: Alfonso Basin, Western Gulf of California and Santa Monica Basin, California Borderland. *Sediment. Geol.* **2000**, *135*, 21–35.
22. Gonzalez-Yajimovich, O.E.; Gorsline, D.S.; Douglas, R.G. Frequency and sources of basin floor turbidites in alfonso basin, Gulf of California, Mexico: Products of slope failures. *Sediment. Geol.* **2007**, *199*, 91–105.
23. Curray, F.; Emmel, J.; Crampton, P.J. Coastal Lagoons: A Symposium. In *Holocene History of a Strand Plain Lagoonal Coast, Nayarit, Mexico*; Ayala-Castanares, A., Ed.; Universidad Nacional Autónoma de México Press: Mexico, Mexico, 1969; pp. 63–10.

24. Gómez-Valdés, J.; Delgado, J.A.; Dworak, J.A. Overtides, compound tides, and tidal-residual current in Ensenada de la Paz lagoon, Baja California Sur, Mexico. *Geofis. Int.* **2003**, *42*, 623–634.
25. Servicio Mareográfico Nacional Universidad Nacional Autónoma de México, Instituto de Geofísica. Available online: <http://www.mareografico.unam.mx/portal/> (accessed on 15 November 2015).
26. Zavala, J. The Head of the Servicio Mareográfico Nacional Universidad Nacional Autónoma de México, Instituto de Geofísica. Personal communication, 2015.
27. Nava-Sanchez, E.H. Modern fan deltas of the west coast of the Gulf of California, Mexico. Ph.D. Thesis, University of Southern California, Los Angeles, CA, USA, 1997.
28. Pérez-Cruz, L.; Urrutia-Fucugauchi, J. Magnetic mineral study of Holocene marine sediments from the Alfonso Basin, Gulf of Mexico-implications for depositional environment and sediment sources. *Geofis. Int.* **2009**, *48*, 305–318.
29. Sánchez-Velasco, L.; Beier, E.; Avalos-García, C.; Lavín, M.F. Larval fish assemblages and geostrophic circulation in Bahía de La Paz and the surrounding southwestern region of the Gulf of California. *J. Plankton Res.* **2006**, *28*, 1081–1098.
30. Oleg Zaytsev, O.; Rabinovich, A.B.; Thompson, R.E.; Silverberg, N. Intense diurnal surface currents in the Bay of LaPaz, Mexico. *Cont. Shelf Res.* **2010**, *30*, 608–619.
31. De Los Monteros, R.L.-E. Evaluating ecotourism in natural protected areas of La Paz Bay, Baja California Sur, Mexico: Ecotourism or nature-based tourism? *Biodivers. Conserv.* **2002**, *11*, 1539–1550.
32. Barr, R.F.; Mourato, S. Investigating the potential for marine resource protection environmental service markets: An exploratory study from La Paz, Mexico. *Ocean Coast. Manag.* **2009**, *52*, 568–577.
33. Servicio, G.M. *Carta Geologic–Minera Coyote G12-D73 Baja California Sur*. Servicio Geológico Mexicano: Pachuca, Mexico, 2008.
34. Trenhaile, A.S.; Porter, N.I.; Prestanski, K. Shore platform and cliff notch transitions along the La Paz Peninsula, southern Baja, Mexico. *Geol. Acta* **2015**, *13*, 167–180.
35. Liu, K.B.; Fearn, M.L. Reconstruction of prehistoric landfall frequencies of catastrophic hurricanes in northwestern Florida from lake sediment records. *Quat. Res.* **2000**, *54*, 238–245.
36. Keen, A.M. *Sea Shells of Tropical West America: Marine Mollusks from Baja California to Peru*, 2nd ed.; Stanford University Press: Stanford, CA, USA, 1971.
37. Reimer, P.J.; Bard, E.; Bayliss A.; Beck, J.W.; Blackwell, P.G.; Bronk Ramsey, C.; Buck, C.E.; Cheng, H.; Edwards, R.L.; Friedrich, M.; *et al.* IntCal13 and MARINE13 radiocarbon age calibration curves 0–50000 years cal BP. *Radiocarbon* **2013**, *55*, 1869–1887.
38. Telford, R.J.; Heegaard, E.; Birks, H.J.B. The intercept is a poor estimate of a calibrated radiocarbon age. *Holocene* **2004**, *14*, 296–298.
39. Frantz, B.R.; Kashgarian, M.; Coale, K.H.; Foster, M.S. Growth rate and potential climate record from a rhodolith using ¹⁴C accelerator mass spectrometry. *Limnol. Oceanogr.* **2000**, *45*, 1773–1777.
40. Engelhart, S.E.; Vacchi, M.; Horton, B.P.; Nelson, A.R.; Kopp, R.E. A sea-level database for the Pacific coast of central North America. *Quat. Sci. Rev.* **2015**, *113*, 78–92.
41. Reynolds, L.C.; Alexander, R.; Simms, A.R. Late Quaternary relative sea level in Southern California and Monterey Bay. *Quat. Sci. Rev.* **2015**, *126*, 57–66.
42. Pillsbury, J. The thorny oyster and the origins of empire: Implications of recently uncovered *Spondylus* imagery from Chan Chan, Peru. *Lat. Am. Antiq.* **1996**, *7*, 313–340.

43. Moore, E.J. *Tertiary Marine Pelecypods of California and Baja California: Nuculidae through Malleidae*; Geological Survey Professional Paper-1228-A; United States Government Printing Office: Washington, DC, USA, 1983.
44. Instituto de Investigaciones Marinas. Available online: <http://institutonazca.org/bivalve-spondylus/> (accessed on 18 July 2015).
45. NOAA Coastal Services Center. Available online: <http://coast.noaa.gov/hurricanes/> (accessed on 9 April 2015).
46. Jien, J.Y.; Gough, W.A.; Butler, K. The influence of El Niño-Southern Oscillation on tropical cyclone activity in the Eastern North Pacific Basin. *J. Clim.* **2015**, *28*, 2459–2474.
47. Jáuregui, E. Climatology of landfalling hurricanes and tropical storms in Mexico. *Atmósfera* **2003**, *16*, 193–204.
48. Rodgers, E.B.; Adler, R.F.; Pierce, H.F. Contribution of tropical cyclones to the North Pacific climatological rainfall as observed from satellites. *J. Appl. Meteorol.* **2000**, *39*, 1658–1678.
49. Romero-Vadillo, E.; Zaytsev, O.; Morales-Pérez, R. Tropical cyclone statistics in the Northeastern Pacific. *Atmósfera* **2007**, *20*, 197–213.
50. Jin, F.F.; Bouchare, J.; Lin, I.I. Eastern Pacific tropical cyclones intensified by El Niño delivery of subsurface ocean heat. *Nature* **2014**, *516*, 82–85.
51. Nanayama, F.; Shigeno, K.; Satake, K.; Shimokawa, K.; Koitabashi, S.; Miyasaka, S.; Ishii, M. Sedimentary differences between the 1993 Hokkaido-nansei-oki tsunami and the 1959 Miyakojima typhoon at Taisei, southwestern Hokkaido, northern Japan. *Sediment. Geol.* **2000**, *135*, 255–264.
52. Bussert, R.; Aberhan, M. Storms and tsunamis: Evidence of event sedimentation in the Late Jurassic Tendaguru Beds of southeastern Tanzania. *J. Afr. Earth Sci.* **2004**, *39*, 549–555.
53. Goff, J.; McFadgen, B.G.; Chagué-Goff, C. Sedimentary differences between the 2002 Easter storm and the 15th-century Okoropunga tsunami, southeastern North Island, New Zealand. *Mar. Geol.* **2004**, *204*, 235–250.
54. Dawson, S. Diatom biostratigraphy of tsunami deposits: Examples from the 1998 Papua New Guinea tsunami. *Sediment. Geol.* **2007**, *200*, 328–335.
55. Morton, R.A.; Gelfenbaum, G.; Jaffe, B.E. Physical criteria for distinguishing sandy tsunami and storm deposits using modern examples. *Sediment. Geol.* **2007**, *200*, 184–207.
56. Goff, J.; Chagué-Goff, C.; Nichol, S.; Jaffe, B.; Dominey-Howes, D. Progress in paleotsunami research. *Sediment. Geol.* **2012**, *243–244*, 70–88.
57. Cuvén, S.; Paris, R.; Falvard, S.; Miot-Niorault, E.; Benbakkar, M.; Schneider, J.-L.; Billy, I. High-resolution analysis of a tsunami deposit: Case-study from the 1755 Lisbon tsunami in southwestern Spain. *Mar. Geol.* **2013**, *337*, 98–111.
58. Donnelly, J.P.; Bryant, S.S.; Butler, J.; Dowling, J.; Fan, L.; Hausmann, N.; Newby, P.; Shuman, B.; Stern, J.; Westover, K.; *et al.* 700 yr sedimentary record of intense hurricane landfalls in southern New England. *Geol. Soc. Am. Bull.* **2001**, *113*, 714–727.
59. Scott, D.B.; Collins, E.S.; Gayes, P.T.; Wright, E. Records of prehistoric hurricanes on the South Carolina coast based on micropaleontological and sedimentological evidence, with comparison to other Atlantic Coast records: *Geol. Soc. Am. Bull.* **2003**, *115*, 1027–1039.
60. Murnane, R.J., Liu, K.-B., Eds. *Hurricanes and Typhoons: Past, Present and Future*; Columbia University Press: New York, NY, USA, 2004.

61. Hippensteel, S.P. Limiting the limits of bioturbation, or at least focusing on the positive. *Palaios* **2005**, *20*, 319–320.
62. Williams, H.F.L. Stratigraphy, sedimentology and microfossil content of Hurricane Rita storm surge deposits in Southwest Louisiana: *J. Coast. Res.* **2009**, *254*, 1041–1051.
63. Williams, H.F.L. Storm surge deposition by Hurricane Ike on the Mcfaddin National Wildlife Refuge, Texas: Implications for paleotempestology studies: *J. Foramin. Res.* **2010**, *40*, 210–219.
64. Hippensteel, S.P. Spatio-lateral continuity of storm overwash deposits in back barrier marshes. *Geol. Soc. Am. Bull.* **2011**, *123*, 2277–2294.
65. Liu, K.-B.; Li, C.; McCloskey, T.A.; Yao, Q.; Weeks, E. Storm deposition in a coastal backbarrier lake in Louisiana caused by hurricanes Gustav and Ike. *J. Coast. Res.* **2011**, *64*, 1866–1870.
66. McCloskey, T.A.; Liu, K.B. A sedimentary-based history of hurricane strikes on the southern Caribbean coast of Nicaragua. *Quat. Res.* **2012**, *78*, 454–464.
67. Kortekaas, S.; Dawson, A.G. Distinguishing tsunami and storm deposits: An example from martinhal, SW Portugal. *Sediment. Geol.* **2007**, *200*, 208–221.
68. Phantuwongraj, S.; Choowong, M.; Nanayama, F.; Hisada, K.-I.; Charusiri, P.; Chutakositkanon, V.; Pailoplee, S.; Chabangbon, A. Coastal geomorphic conditions and styles of storm surge washover deposits from Southern Thailand. *Geomorphology* **2013**, *192*, 43–58.
69. Moy, C.M.; Seltzer, G.O.; Rodbell, D.T.; Anderson, D.M. Variability of El Nino/Southern Oscillation activity at millennial timescales during the Holocene epoch. *Nature* **2002**, *420*, 162–165.
70. Staines-Urias, F.; Gonzalez-Yajimovich, O.; Beaufort, L. Reconstruction of past climate variability and ENSO-like fluctuations in the southern Gulf of California (Alfonso Basin) since the last glacial maximum. *Quat. Res.* **2015**, *83*, 488–501.
71. Jankaew, K.; Atwater, B.F.; Sawai, Y.; Choowang, M.; Charoentitirat, T.; Prendergast, A.; Martin, M.E.; Medieval forewarning of the 2004 Indian Ocean tsunami in Thailand. *Nature* **2008**, *455*, 1228–1231.
72. Soria, J.; Switzer, A.; Villanoy, C.; Fritz, H.; Bilgera, P.; Cabrera, O.; Siringan, F.; Sta Maria, Y.; Ramos, R.; Fernandez, I. Repeat storm surge disasters of Typhoon Haiyan and its 1897 predecessor in the Philippines. *Bull. Am. Meteor. Soc.* **2015**, in press.
73. U.S. National Earthquake Data Center. Available online: <http://earthquake.usgs.gov/earthquakes/search> (accessed on 10 July 2015).
74. DeLange, W.P.; Moon, V.G. Tsunami washover deposits, Tawharanui, New Zealand. *Sediment. Geol.* **2007**, *200*, 232–247.